PNAS
www.pnas.org

Supplementary Information for

Early sarcomere and metabolic defects in a zebrafish *pitx2c* cardiac arrhythmia model

Michelle M. Collins[1], Gustav Ahlberg, Camilla Vestergaard Hansen, Stefan Guenther, Rubén Marín-Juez, Anna M. Sokol, Hadil El-Sammak, Janett Piesker, Ylva Hellsten, Morten S. Olesen, Didier Y. R. Stainier[1], Pia R. Lundegaard[1]

[1] Authors for Correspondence:

Michelle M. Collins, PhD
Email: Michelle.Collins@mpi-bn.mpg.de

Didier Y.R. Stainier, PhD
Email: Didier.Stainier@mpi-bn.mpg.de

Pia R. Lundegaard, PhD
Email: plundegaard@sund.ku.dk

This PDF file includes:

Supplementary Information Text
Figures S1 to S8
Table S1
Legends for Movies S1 to S4
SI References

Other supplementary materials for this manuscript include the following:

Movies S1 to S4

Supplementary Information Text

EXTENDED METHODS

Zebrafish husbandry

The following mutant and transgenic lines were used in this study: *pitx2c*^{ups6} (1), *Tg(myl7:LIFEACT-GFP)*^{s974Tg} (2) (abbreviated at *Tg(myl7:LA-GFP)*), *Tg(myl7:MKATE-CAAX)*^{sd11Tg} (3), *Tg(myl7:actn3b-EGFP)*^{sd10Tg} (3), *Tg(myl7:MITO-roGFP2-Sce.Hyr1)*^{uto54Tg} (4) (referred to as *Tg(myl7:MITO-roGFP2-Orp1)*), *mia40a*^{bns292} (5), and *ppargc1a*^{bns176} (Marin-Juez et al., in press). The *Tg(myl7:pitx2c-P2A-H2BGFP)* line was generated by cloning the full-length *pitx2c* coding sequence upstream of a P2A linker and nuclear-targeted GFP sequence. This cassette was then cloned downstream of the 0.8 kb *myl7* promoter sequence with flanking Tol2 sites. F0 adult fish were outcrossed to obtain F1 embryos used for imaging, RNA-seq experiments, and qPCR. F1 offspring survive until ~ 5 days post-fertilization (dpf).

ECG analysis

The fish were orally perfused with fish tank water containing 0.03% Tricaine using a roller pump (ISM827B, ISMATEC Germany) at 2 ml/minute. Two custom-made stainless-steel electrodes were placed on top or slightly subcutaneously above the cardiac region using micromanipulators (Marzhauser MM33, Marzhauser Germany). The electrodes were connected to a differential AC amplifier (A-M Systems, WA, USA) with the following filter settings: Low cut-off filter =10 Hz; high cut-off filter = 1 KHz; Gain = x100. Signals were digitized in a PowerLab 4/30 (AD instruments, USA) and recorded at 10 k/s in LabChart 7.0 (AD Instruments, USA) using a digital low pass filter (cut-off frequency = 50 Hz; active input amplifier = 5 V range; low pass filter = 200 Hz; Mains filter = active).

Echocardiography

Echocardiography was performed using the Vevo2100 Imaging System (VisualSonics) equipped with a high frequency transducer MS700 (40 MHz). Adult fish were anesthetized in 0.01% Tricaine, fixed in modelling clay and submerged in system water with Tricaine. Long axis views were obtained by positioning the transducer on the ventral surface along the cranial-caudal axis until both chambers were in view. Pulsed-wave Doppler (PWD) measurements were recorded at the atrioventricular valve region, where maximum flow velocity was detected. Both B-Mode and PWD signals were recorded for 3-5 s, and movies were recorded three times per fish. Measurements and analysis were performed using VevoLab software package (VisualSonics). Systolic and diastolic longitudinal ventricular area and length were measured to calculate fractional area change and fractional shortening. Measurements were averaged from three cardiac cycles taken from at least two recordings per fish.

Transmission electron microscopy

Adult *pitx2c*$^{+/+}$ and *pitx2c*$^{-/-}$ hearts were dissected from 18 mpf zebrafish and fixed in 4% paraformaldehyde with 2.5% glutaraldehyde in 0.05 M HEPES buffer (pH 7.2) for 2 hr at room temperature, and subsequently stored at 4°C. Samples were rinsed three times in 0.05 M HEPES buffer (pH 7.2), post fixed in 1% (w/v) OsO_4 in distilled water for 1 hr, washed three times with distilled water, and followed by en bloc staining with 2% uranyl acetate in distilled water for 1 hr. Samples were dehydrated through a graded series of ethanol washes, transferred to propylene oxide and embedded in Epon according to standard procedures. Embryonic samples were collected at 56 hpf and fixed in ice-cold 1% paraformaldehyde, 2% glutaraldehyde in 0.1 M sodium cacodylate buffer (pH 7.4) for 30 min on ice and store at 4°C overnight. The lower third of the

trunk was removed and used for genotyping. Samples were washed in 0.1 M sodium cacodylate buffer and post fixed in 2% OsO_4, followed by en block staining (2% uranyl acetate in distilled water, 1 hr). Samples were dehydrated through a graded series of acetone washes, transferred to an acetone/Epon solution, and embedded in Epon. Sections from both adult and embryonic tissue were cut approximately 70 nm thick with a Reichert-Jung Ultracut E microtome and collected on copper grids. Sections were examined with a Jeol JEM-1400 Plus transmission electron microscope (Jeol, Japan), operated at an accelerating voltage of 120 kV. Digital images were recorded with an EM-14800 Ruby Digital CCD camera unit (3296px x 2472px).

Confocal microscopy and analysis of cardiac arrhythmia

Live zebrafish were anesthetized with 0.004% Tricaine and mounted in 1% low-melting agarose in egg water containing Tricaine for confocal imaging. Stopped hearts were imaged using Zeiss LSM800 or LSM880 upright laser scanning confocal microscopes with a Plan-Apochromat 20x/40x dipping lens. Live imaging of beating hearts was performed using a Zeiss spinning disk confocal microscope. Larvae were mounted in 1-2% low-melting agarose without Tricaine. 20-30 s movies were recorded with 5 ms exposure. Light intensity and duration were kept to a minimum to avoid light-induced arrhythmias and twitching. Kymographs were generated using ImageJ. To determine cardiac cycles, a pixel intensity profile was measured across the kymograph and imported into MATLAB to smoothen and identify peaks. Root mean square of the successive differences (RMSSD) was obtained by calculating the successive time differences between 8-10 cardiac cycles in milliseconds (ms) according to the following formula:

$$\text{RMSSD} = \sqrt{\frac{1}{N-1}\left(\sum_{i-1}^{N-1}((R-R)_{i+1} - (R-R)_i)^2\right)}$$

RNA-sequencing and pathway analysis

Total RNA was isolated from 56 hpf embryonic hearts using the RNeasy Micro kit (Qiagen). For exclusion of genomic DNA contamination, the samples were treated by on-column DNase digestion (DNase-Free DNase Set, Qiagen). Total RNA and library integrity were verified with LabChip Gx Touch 24 (Perkin Elmer). 5 ng of total RNA was used as input for SMARTer® Stranded Total RNA-Seq Kit - Pico Input Mammalian (Takara Clontech). Sequencing was performed on the NextSeq500 instrument (Illumina) using v2 chemistry, resulting in an average of 33M reads per library with 1x75bp single end setup. The resulting raw reads were assessed for quality, adapter content and duplication rates with FastQC (available online at: http://www.bioinformatics.babraham.ac.uk/ projects/fastqc). Reaper version 13-100 was employed to trim reads after a quality drop below a mean of Q20 in a window of 10 nucleotides (6). Only reads between 30 and 150 nucleotides were cleared for further analyses. Trimmed and filtered reads were aligned versus the Ensembl Zebrafish genome version DanRer10 (GRCz10.87) using STAR 2.4.0a with the parameter "--outFilterMismatchNoverLmax 0.1" to increase the maximum ratio of mismatches to mapped length to 10% (7). The number of reads aligning to genes was counted with featureCounts 1.4.5-p1 tool from the Subread package (8). Only reads mapping at least partially inside exons were admitted and aggregated per gene. Reads overlapping multiple genes or aligning to multiple regions were excluded. The Ensembl annotation was enriched with UniProt data (release 06.06.2014) based on Ensembl gene identifiers (Activities at the Universal Protein Resource (UniProt)). Demultiplexing of RNA-seq data and conversion of the bcl file format to the fastq file format was made with the Illumina CASAVA v1.8 software. To quantify RNA-seq transcript expression, Salmon v0.11.3 (9) was used to perform quasi mapping of raw reads to the GRCz10 (Genome Reference Consortium, accessed 19.11.2018) transcriptome, with settings

specified for GC- and sequence-specific biases. RNA-seq datasets have been deposited to the GEO repository under the accession number GSE128511.

Differential expression (DE) analysis was performed with R-package DESeq2 (10). Gene level count matrices were created from the transcript level quantifications, obtained from quasi-mapping, and using the tximport (11) R-package. Significance of DE was assessed with Wald test and *P*-values were adjusted for multiple testing by Independent Hypothesis Weighting (12). An adjusted *P*-value >0.05 was considered significant. Log fold change (LFC) estimated effect size were shrunk using the DESeq2 function lcfShrink. Gene Set Enrichment Analysis (GSEA) of Kyoto Encyclopedia of Genes and Genome (KEGG) pathways was performed in the R-package fgsea (13-15). In order to avoid sample source bias, a background gene set with genes that had normalized count >15 in 2 or more samples was defined (16). Genes were ranked by the -log10 of *P*-values and the direction of the LFC, assigning downregulated genes a negative value and upregulated a positive value. Gene set enrichments with a Benjamini & Hochberg adjusted *P*-value <0.01 were considered significant.

Measurement of mitochondrial respiration and reactive oxygen species (ROS)

Mitochondrial capacity and ROS production were measured in the Oxygraph-2k (O2k) for high-resolution FluoRespirometry (Oroboros Instruments, Innsbruck, Austria). For analysis of H_2O_2 emission, the O2k was used in combination with O2k-Fluorescence LED2-Modules (Fluorescence-Sensor Green 525 nm) and Amplex UltraRed, which enables measurement of respiration and H_2O_2 emission simultaneously (17). Cardiac chambers from 6 mpf *pitx2c*$^{+/+}$ and *pitx2c*$^{-/-}$ were analyzed separately in pools of four atria or of two ventricles. Immediately after dissection, the atria and ventricles were placed in ice cold relaxing buffer (Buffer X: 60 mM K-MES, 35 mM KCl, 7.23 mM K_2EGTA, 2.77 mM CaK_2EGTA, 20 mM Imidazole, 0.5 mM DTT, 20 mM Taurine, 5.7 mM Na_2ATP, 15 mM Na_2PCr and 6.56 mM $MgCl_2 \cdot 6H_2O$ adjusted to pH 7.1 with 5M KOH at 0°C) for preservation of cardiac muscle fibers for analysis of mitochondrial respiratory capacity and H_2O_2 emission. The cardiac muscle fibers were analyzed for mitochondrial respiratory capacity as described for skeletal muscle fibers (18, 19). In brief, the atria and ventricles were dissected on ice and permeabilized with a mild detergent (Saponin 50 µg/ml Buffer X) for 30 min. The preparations were washed twice for 10 min in emission media (Buffer Z: 1mM EGTA, 5mM $MgCl_2 \cdot 6H_2O$, 105mM K-MES, 30 mM KCl, 10 mM KH_2PO4 and 5 mg/ml BSA (fatty acid free) adjusted to pH 7.1 with 10 M KOH at 37°C). The permeabilization and washing procedures were performed on ice on an orbital shaking platform.

O2k and Amplex UltraRed analyses were carried out in duplicates, in hyperoxia conditions (i.e. between 200-450 µM O_2) with a chamber temperature of 37°C in Buffer Z. For measurement of H_2O_2 emission capacity, blebbistatin, superoxide dismutase (SOD) and Amplex UltraRed (25 µM, 5U·ml-1, 10 µM) were added to the chambers followed by horseradish peroxidase (HRP; 1U·ml-1). Addition of HRP catalyzes the oxidation of Amplex UltraRed by H_2O_2 to the fluorescent compound resofurin. Hereafter, glutamate and malate (10 and 2 mM) were added to assess Complex I leak respiration and H_2O_2 emission and subsequently succinate (1 and 10 mM) was added to determine Complex I&II leak respiration and H_2O_2 emission. ADP (5 mM) was added to measure maximal oxidative phosphorylation capacity. Before every substrate titration and after the last substrate titration, H_2O_2 (0.1 µM) was added for calibration of the sensitivity decline of the sensor during the experiment (17).

Histology analysis and imaging

3 and 14 mpf zebrafish hearts were fixed overnight in 4% paraformaldehyde at 4°C. Hearts were washed with PBS, cryopreserved with sucrose, embedded in OCT (Tissue-Tek) and stored at -80°C. Cryosections were cut at 10-12 µm and collected on Superfrost slides. Staining for fibrosis was performed using an AFOG staining kit, and hematoxylin and eosin staining was performed according to standard protocols. Imaging of sections was performed using a Zeiss stereomicroscope or Nikon SMZ25 stereomicroscope.

qPCR and mtDNA analysis

Total RNA was isolated from pools of 25 dissected embryonic hearts at 56 hpf or pools of 4 adult atria at 8 mpf using the RNeasy Micro kit with on-column DNase treatment (Qiagen) following manufacturer's instructions. cDNA was synthesized with Maxima First Strand synthesis (ThermoFisher) and qPCR was performed using a BioRad CFX Connect Real-Time System. Expression levels were normalized to the expression of *rpl13a*. Relative mitochondrial DNA levels were quantified as described (5). Primer sequences and average Ct values are provided in Table S1.

Chemical treatment

Larvae were exposed to 100 µM N-acetyl cysteine (A7250, Sigma) in egg water. Solutions were changed daily or washed out according to dosage scheme.

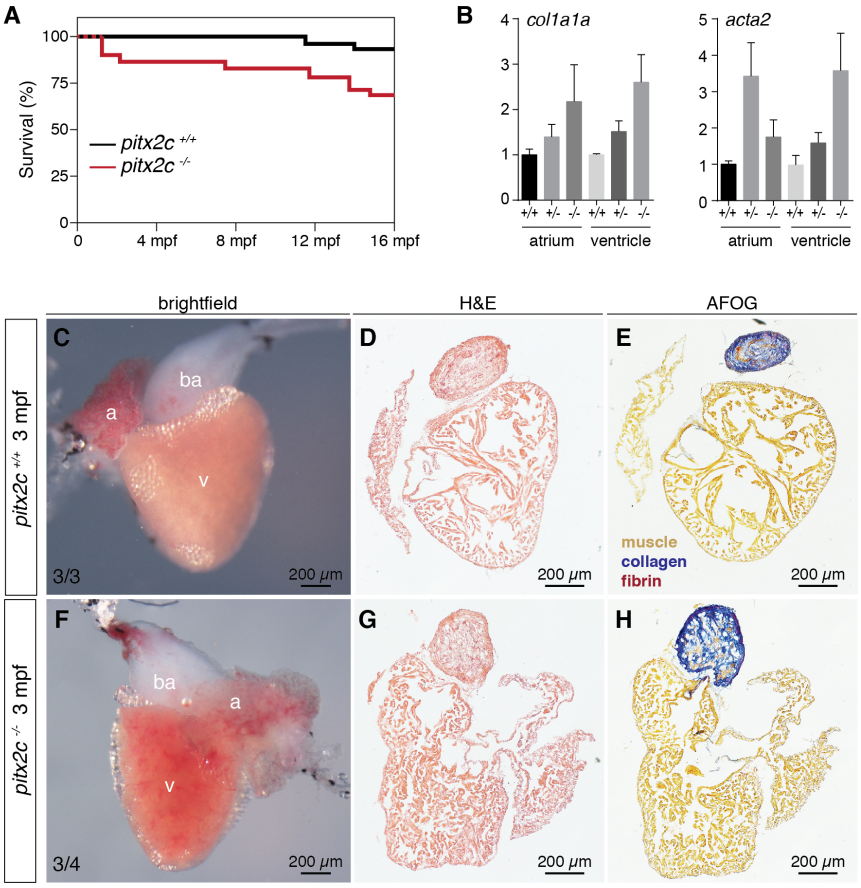

Fig. S1. Analysis of survival and fibrosis in *pitx2c*$^{-/-}$ juveniles and adults.
(A) Survival curve of *pitx2c*$^{+/+}$ (black line) and *pitx2c*$^{-/-}$ (red line) siblings. *(B)* qPCR analysis of *col1a1* and *acta2* mRNA levels. Error bars correspond to SEM. *(C-H)* Cardiac morphology in *pitx2c*$^{+/+}$ *(C-E)* and *pitx2c*$^{-/-}$ *(F-H)* zebrafish at 3 mpf. Whole-mount brightfield images of the heart *(C, D)*. Tissue structure was examined by H&E staining *(D, G)* and for the presence of fibrosis by AFOG staining *(E, H)*. Atrial hypertrophy is evident in *pitx2c*$^{-/-}$ hearts at 3 mpf, while the presence of fibrosis was not detected in any of the hearts examined (n=4).

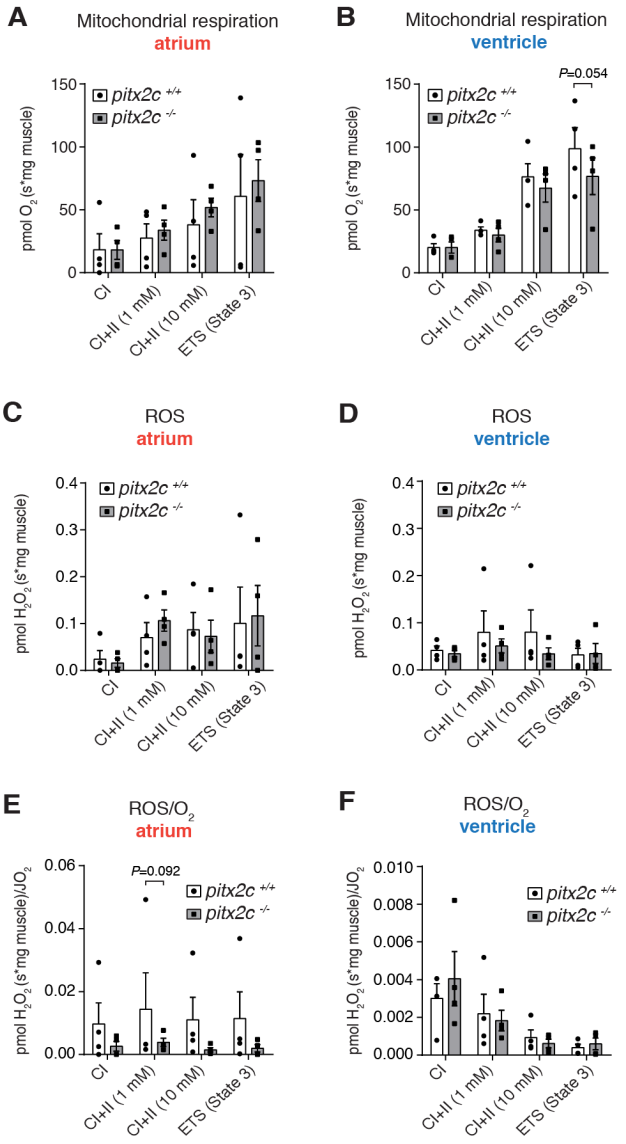

Fig. S2. Analysis of mitochondrial bioenergetics in *pitx2c*$^{-/-}$ adult hearts.
Mitochondrial bioenergetics analysis from pools of adult atria *(A, C, E)* and ventricles *(B, D, F)*. *(A, B)* Mitochondrial respiration in atria or ventricles from *pitx2c*$^{+/+}$ and *pitx2c*$^{-/-}$ siblings. Maximal oxidative phosphorylation capacity (ETS State 3) is slightly elevated in *pitx2c*$^{-/-}$ atria *(A)* while reduced in *pitx2c*$^{-/-}$ ventricles *(B)* compared to *pitx2c*$^{+/+}$ siblings. *(C, D)* Total ROS levels in atria or ventricles from *pitx2c*$^{+/+}$ and *pitx2c*$^{-/-}$ siblings. *(E, F)* ROS levels normalized to O_2 respiration levels in atria or ventricles from *pitx2c*$^{+/+}$ and *pitx2c*$^{-/-}$ siblings. Error bars correspond to SEM; $P < 0.05$ (*) by linear regression analysis. CI, Complex I; CII, Complex II; ETS, electron transfer system.

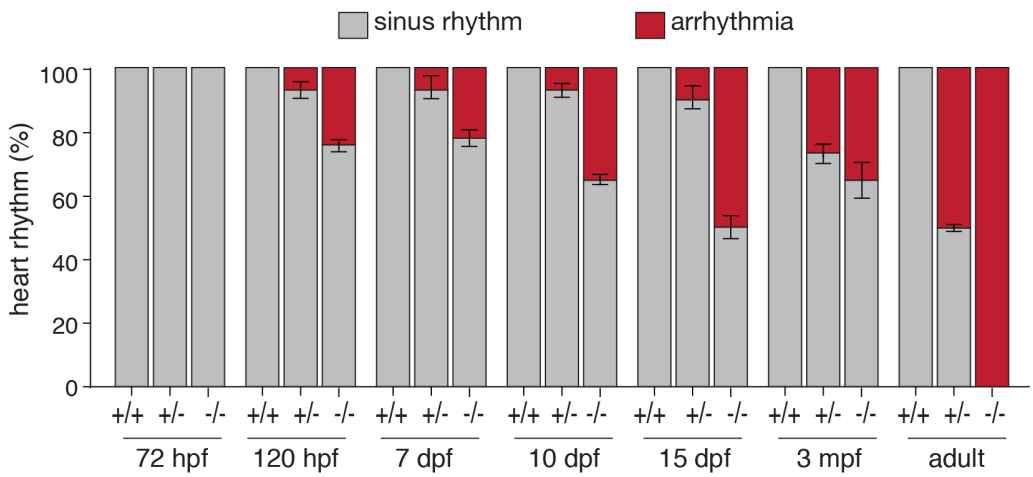

Fig. S3. Cardiac arrhythmia is observed in *pitx2c*$^{-/-}$ at developmental and adult stages. Incidence of cardiac arrhythmia in larval, juvenile, and adult *pitx2c*$^{+/+}$, *pitx2c*$^{+/-}$, and *pitx2c*$^{-/-}$ zebrafish. Bar graphs show the proportion of animals scored for sinus rhythm (gray) or arrhythmia (red). Phenotype scoring for 3 mpf and adults was performed by echocardiography or ECG. n > 10 fish per genotype/stage.

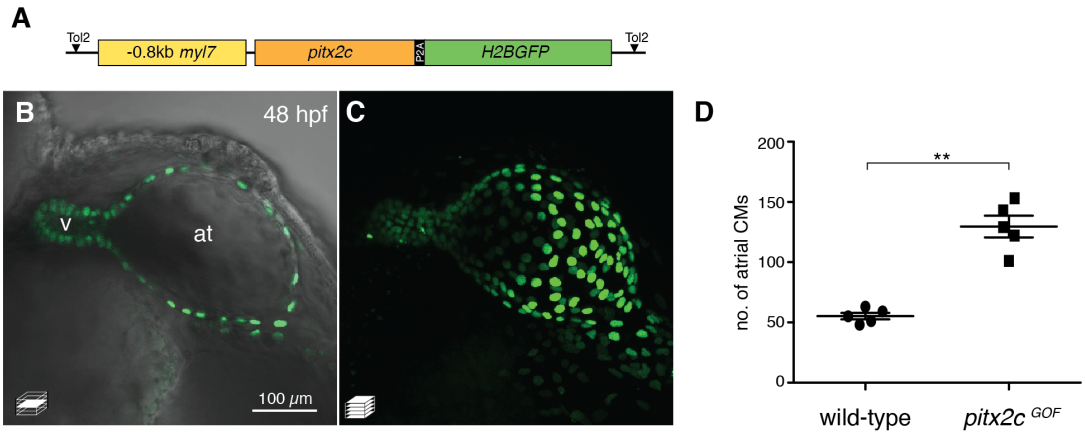

Fig. S4. Generation of a *pitx2c* overexpression line.
(A) Schematic of the construct designed to overexpress *pitx2c* under control of the *myl7* promoter, *myl7:pitx2c-P2A-H2BGFP* (referred to as *pitx2c*^{GOF}). *(B, C)* Cardiac morphology of the *pitx2c*^{GOF} line at 48 hpf; embryos exhibit an enlarged atrium and collapsed ventricle. *(D)* Quantification of atrial cardiomyocyte (CM) number in 48 hpf *Tg(myl7:pitx2c-P2A-H2BGFP)* embryos. at, atrium; v, ventricle. Error bars correspond to SEM. $P < 0.01$ (**) by unpaired *t*-test.

A

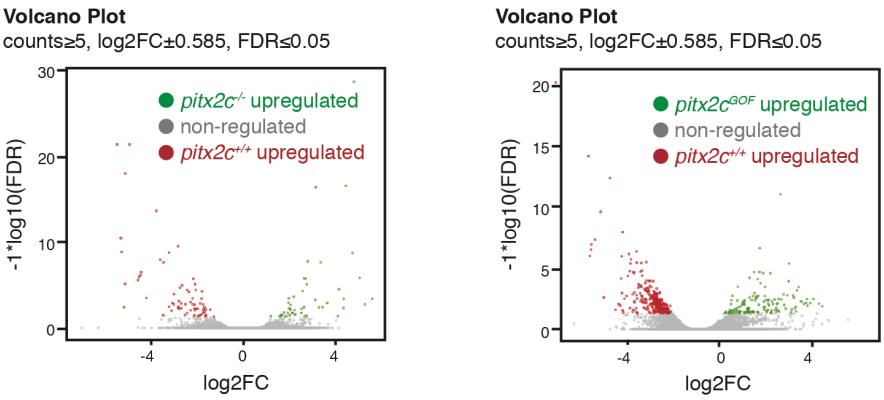

B

GSEA KEGG pathways - *pitx2c*$^{-/-}$ *vs pitx2c*$^{+/+}$ 56 hpf hearts

Pathway	Gene Ranks	NES	padj
Oxidative phosphorylation		-2.63	3.4e-03
Carbon metabolism		-2.12	3.4e-03
Cardiac muscle contraction		-2.28	3.4e-03

C

GSEA KEGG pathways - *pitx2c*^{GOF} *vs pitx2c*$^{+/+}$ 56 hpf hearts

Pathway	Gene Ranks	NES	padj
Oxidative phosphorylation		-2.53	1.3e-03
Carbon metabolism		-2.33	1.3e-03
Cardiac muscle contraction		-2.24	1.3e-03
Biosynthesis of amino acids		-2.09	1.3e-03
Gycolysis/Gluconeogenesis		-2.29	1.3e-03
Valine, leucine and isoleucine degradation		-1.98	1.3e-03
Pyruvate metabolism		-1.95	1.9e-03
DNA replication		-1.93	1.9e-03
Citrate cycle (TCA)		-1.96	1.9e-03
Fatty acid degradation		-1.93	2.5e-03

D

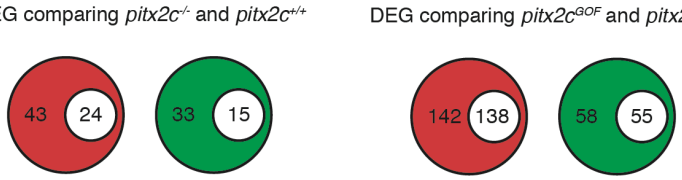

Fig. S5. RNA-seq analysis from *pitx2c*$^{-/-}$ and *pitx2c*^{GOF} hearts reveals changes in cardiac sarcomere function and metabolic pathways.
(A) Volcano plots showing differentially expressed genes in 56 hpf hearts comparing *pitx2c*$^{-/-}$ vs *pitx2c*$^{+/+}$ and *pitx2c*^{GOF} vs *pitx2c*$^{+/+}$ RNA-seq datasets using a log2 fold change (FC) of ± 0.585 with a false discovery rate (FDR) of ≤ 0.05. *(B, C)* Gene set enrichment analysis (GSEA) showing KEGG pathways comparing *pitx2c*$^{-/-}$ vs *pitx2c*$^{+/+}$ hearts *(B)* and *pitx2c*^{GOF} vs *pitx2c*$^{+/+}$ hearts *(C)* at 56 hpf. KEGG pathways in green are represented in both datasets. NES, normalized enrichment score. *(D)* Differentially expressed genes (DEG) were cross-referenced with ChIP-seq data from *Pitx2-Flag* mouse neonatal ventricles (20). Red circles indicate the number of downregulated genes, green circles indicate the number of upregulated genes. White circles indicate the number of DEGs for which a PITX2 ChIP-seq peak assigned to the mouse orthologous gene was identified.

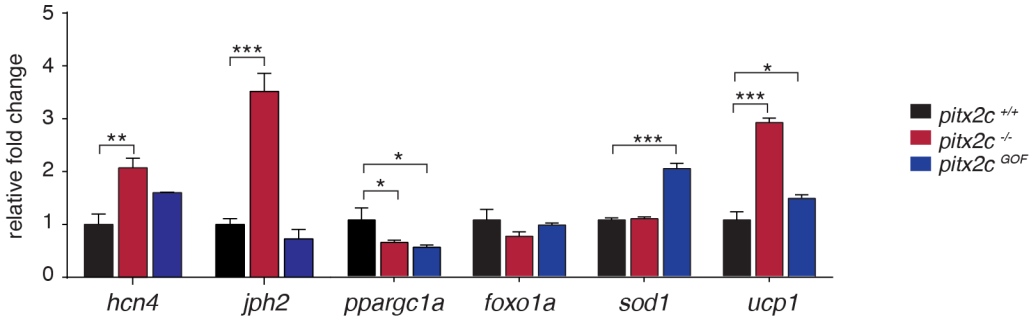

Fig. S6. Validation of differentially expressed genes from RNA-seq analysis of embryonic hearts.

qPCR performed using dissected hearts from 56 hpf *pitx2c*$^{+/+}$ (black bars), *pitx2c*$^{-/-}$ (red bars), and *pitx2c*^{GOF} (blue bars) embryos. Error bars correspond to SEM; $P < 0.05$ (*), $P < 0.01$ (**), $P < 0.001$ (***) by unpaired *t*-test.

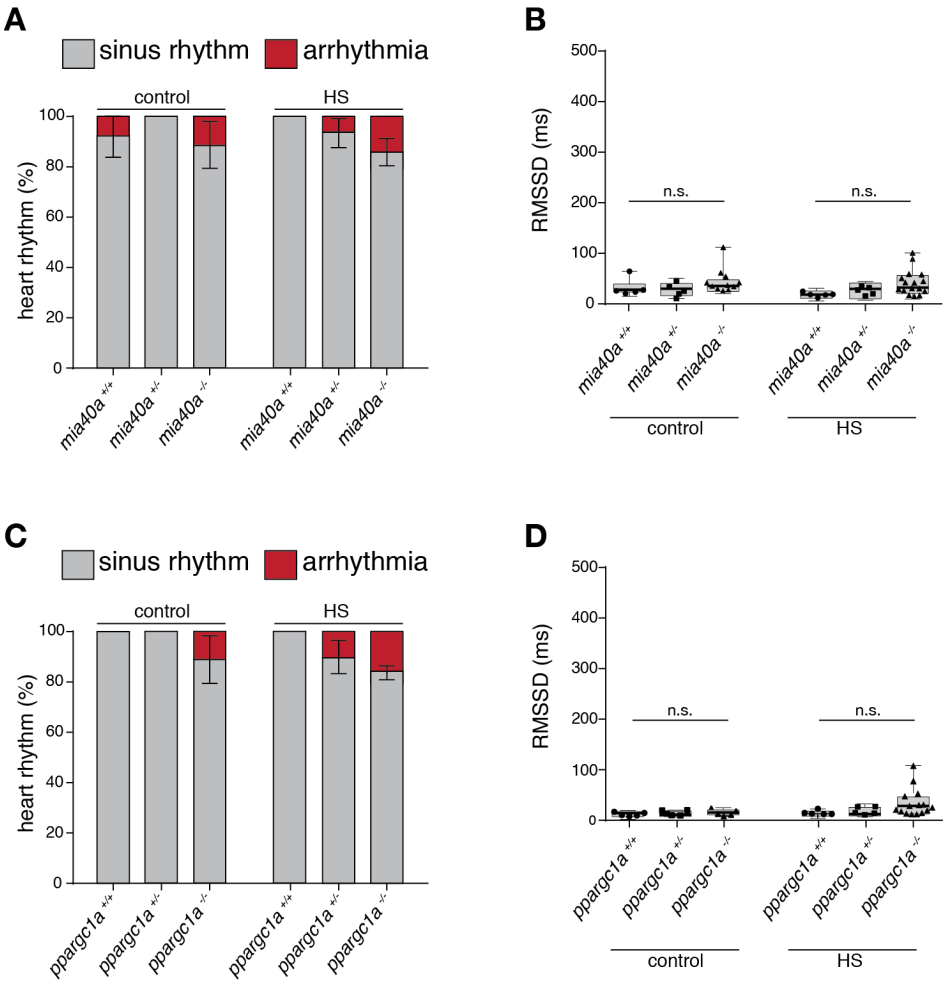

Fig. S7. Analysis of cardiac arrhythmia in larval zebrafish models of metabolic dysfunction. *(A-D)* Larvae from incrosses of *mia40a*$^{+/-}$ *(A, B)* or *ppargc1a*$^{+/-}$ *(C, D)* fish were scored for cardiac rhythm at 120 hpf in control conditions or following a 1 hr heat shock (HS) prior to imaging. Box-and-whisker plots of RMSSD scores *(B, D)* from *mia40a*$^{+/-}$ and *ppargc1a*$^{+/-}$ incrosses in control conditions or following HS treatment. No significant differences were observed across the genotypes or following HS for *mia40a* or *ppargc1a*, suggesting that metabolic dysfunction alone is insufficient to induce cardiac arrhythmia. Each data point represents the average interval calculated from 8-10 cardiac cycles of individual larvae. Gray bars indicate normal sinus rhythm; red bars indicate arrhythmia. n > 20 larvae per genotype. Error bars correspond to SEM from 3 independent experiments.

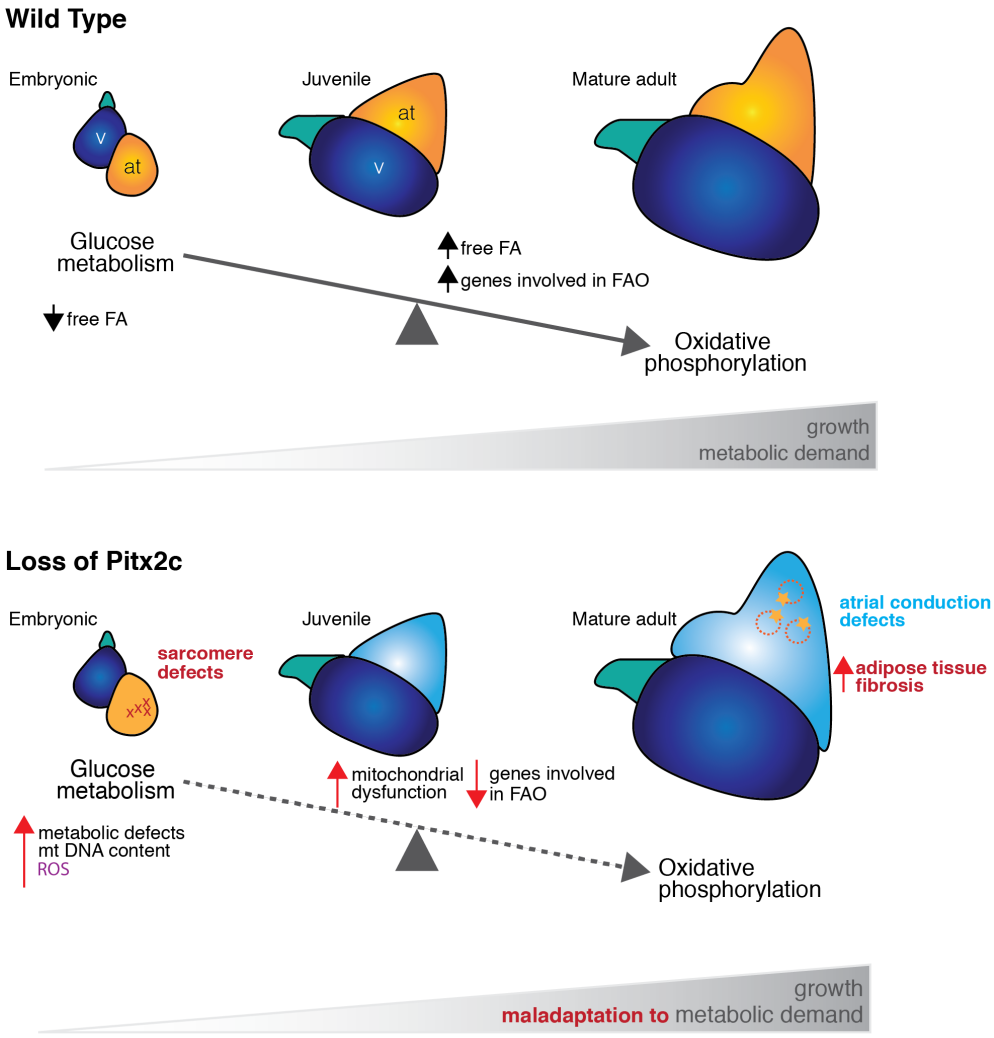

Fig. S8. Proposed model of Pitx2c function in the heart.
We propose a model whereby sarcomere and metabolic defects present in the *pitx2c*$^{-/-}$ embryonic heart act as arrhythmogenic substrates already at early developmental stages. During adult stages, conduction defects, mitochondrial dysfunction, and structural remodeling are observed in *pitx2c*$^{-/-}$ atria. We hypothesize that the pathogenesis of arrhythmia and AF-like phenotypes in *pitx2c*$^{-/-}$ is driven by the early sarcomere and metabolic dysfunction that leads to cardiomyopathy and altered cardiac energetics. v, ventricle; at, atrium; FA, fatty acids; FAO, fatty acid oxidation; ROS, reactive oxygen species.

Table S1. qPCR oligos and average Ct values

	Forward oligo	Reverse oligo	Avg. Ct
cox7c	CTGAAAACAATGCTCGGACA	AATCCACTGCCGAAGAACAG	19.56
ppargc1a	CTGAAGAAGCTCCTCCTGGC	CCTCGTGGTTTGCTGTTCCA	22.71
ppargc1b	GCATTGTTGAGGACGGAGTC	TTAGGGGGTGTCAACAGGAG	24.28
esrra	TACAAGAGACGCCCTGAGGT	GCCAGGTCACAGAGAGTGGT	23.11
foxo1a	ACCTGATCACCAAAGCCATC	CTCATTCTGCACTCGGATGA	24.62
pparaa	CGACAAGTGTGAACGCAACT	GCTTCTCGGACTGGGGTATC	23.17
sod1	GCACTTCAACCCTCATGACA	CGGTCACATTACCCAGGTCT	19.26
sod2	GAGCCTCACATCTGTGCTGA	ATTTCAATGCAGGCTGAAGG	19.68
nrf1	TAGGCCAGCAGGCTATTGTT	CGTTTTCCAGATCCTCCAGA	24.03
ucp1	AGGAACGCTCTGGTCAACTG	TACCACATCCACAGGAGACG	20.11
mcu	AGTGACACGGTGGGTGTTTT	CCCTGTTGAGGACGCTATTC	20.70
prdx5	GCCTCTCAATGGCTGAACTC	GCAACCTCATCCACACCTTT	20.94
fabp11a	GCACCTTCAAAACCACCGAG	TATTGTGGACTCCTTGCCGT	25.63
adipor2	TGCTCCCTGATTGGCTGAAG	CACGATGCCCAGACAGAGAA	28.99
zbtb16b	ACATCTGCAGCGAGTGTGAA	CCTTCAATGTGCTCTCGTCA	29.42
jph2	GTCCAGTATCGCTCGAGTGG	CAACAAGGGCTCGTGAATGC	22.21
cola1a1	GTACTGGATTGACCCTGACC	CATACTCGAACTGGAAGCCA	29.66
acta2	GAAGATCAAGATAATCGCTCCAC	GCAATAGCAGAATTACGGGAC	23.65
rpl13a	TCTGGAGGACTGTAAGAGGTATGC	AGACGCACAATCTTGAGAGCAG	16.12

***** average Ct values were calculated from 3 biological replicates of *pitx2c*$^{+/+}$ atria.

LEGENDS FOR MOVIE FILES

Movie S1: B-Mode echocardiography of cardiac function in a *pitx2c*$^{+/+}$ sibling at 8 mpf.

Movie S2: B-Mode echocardiography of cardiac function in a *pitx2c*$^{-/-}$ sibling at 8 mpf.

Movie S3: Spinning disk confocal imaging of a 120 hpf *pitx2c*$^{+/+}$ larva scored as sinus rhythm.

Movie S4: Spinning disk confocal imaging of a 120 hpf *pitx2c*$^{-/-}$ larva scored as arrhythmic.

SI APPENDIX REFERENCES

1. Collins MM*, et al.* (2018) Pitx2c orchestrates embryonic axis extension via mesendodermal cell migration. *eLife* 7.
2. Reischauer S, Arnaout R, Ramadass R, & Stainier DY (2014) Actin binding GFP allows 4D in vivo imaging of myofilament dynamics in the zebrafish heart and the identification of Erbb2 signaling as a remodeling factor of myofibril architecture. *Circ Res* 115(10):845-856.
3. Lin YF, Swinburne I, & Yelon D (2012) Multiple influences of blood flow on cardiomyocyte hypertrophy in the embryonic zebrafish heart. *Dev Biol* 362(2):242-253.
4. Panieri E, Millia C, & Santoro MM (2017) Real-time quantification of subcellular H2O2 and glutathione redox potential in living cardiovascular tissues. *Free radical biology & medicine* 109:189-200.
5. Sokol AM*, et al.* (2018) Loss of the Mia40a oxidoreductase leads to hepato-pancreatic insufficiency in zebrafish. *PLoS genetics* 14(11):e1007743.
6. Davis MP, van Dongen S, Abreu-Goodger C, Bartonicek N, & Enright AJ (2013) Kraken: a set of tools for quality control and analysis of high-throughput sequence data. *Methods* 63(1):41-49.
7. Dobin A*, et al.* (2013) STAR: ultrafast universal RNA-seq aligner. *Bioinformatics* 29(1):15-21.
8. Liao Y, Smyth GK, & Shi W (2014) featureCounts: an efficient general purpose program for assigning sequence reads to genomic features. *Bioinformatics* 30(7):923-930.
9. Patro R, Duggal G, Love MI, Irizarry RA, & Kingsford C (2017) Salmon provides fast and bias-aware quantification of transcript expression. *Nat Methods* 14(4):417-419.
10. Love MI, Huber W, & Anders S (2014) Moderated estimation of fold change and dispersion for RNA-seq data with DESeq2. *Genome Biol* 15(12):550.
11. Soneson C, Love MI, & Robinson MD (2015) Differential analyses for RNA-seq: transcript-level estimates improve gene-level inferences. *F1000Res* 4:1521.
12. Ignatiadis N, Klaus B, Zaugg JB, & Huber W (2016) Data-driven hypothesis weighting increases detection power in genome-scale multiple testing. *Nat Methods* 13(7):577-580.
13. Subramanian A*, et al.* (2005) Gene set enrichment analysis: a knowledge-based approach for interpreting genome-wide expression profiles. *Proc Natl Acad Sci U S A* 102(43):15545-15550.
14. Sergushichev A (2016) An algorithm for fast preranked gene set enrichment analysis using cumulative statistic calculation. *bioRxiv*:060012.
15. Kanehisa M, Furumichi M, Tanabe M, Sato Y, & Morishima K (2017) KEGG: new perspectives on genomes, pathways, diseases and drugs. *Nucleic Acids Res.* 45(D1):D353-d361.
16. Simillion C, Liechti R, Lischer HE, Ioannidis V, & Bruggmann R (2017) Avoiding the pitfalls of gene set enrichment analysis with SetRank. *BMC Bioinformatics* 18(1):151.
17. Krumschnabel G*, et al.* (2015) Simultaneous high-resolution measurement of mitochondrial respiration and hydrogen peroxide production. *Methods Mol Biol* 1264:245-261.
18. Pesta D & Gnaiger E (2012) High-resolution respirometry: OXPHOS protocols for human cells and permeabilized fibers from small biopsies of human muscle. *Methods Mol Biol* 810:25-58.
19. Komlodi T*, et al.* (2018) Comparison of Mitochondrial Incubation Media for Measurement of Respiration and Hydrogen Peroxide Production. *Methods Mol Biol* 1782:137-155.
20. Tao G*, et al.* (2016) Pitx2 promotes heart repair by activating the antioxidant response after cardiac injury. *Nature* 534(7605):119-123.